ResearchGate

See discussions, stats, and author profiles for this publication at: https://www.researchgate.net/publication/263335478

Ln-MOF Pseudo-Merohedral Twinned Crystalline Family as Solvent-Free Heterogeneous Catalysts

ARTICLE *in* CRYSTAL GROWTH & DESIGN · MARCH 2014

Impact Factor: 4.89 · DOI: 10.1021/cg5002336

CITATIONS
2

READS
30

5 AUTHORS, INCLUDING:

Richard Fernando D'vries
University of São Paulo
21 PUBLICATIONS **152** CITATIONS
SEE PROFILE

Enrique Gutiérrez-Puebla
Instituto de Ciencia de Materiales de Madrid
346 PUBLICATIONS **6,125** CITATIONS
SEE PROFILE

Angeles Monge
Spanish National Research Council
441 PUBLICATIONS **6,771** CITATIONS
SEE PROFILE

Available from: Richard Fernando D'vries
Retrieved on: 03 February 2016

CRYSTAL GROWTH & DESIGN

Article

pubs.acs.org/crystal

Ln-MOF Pseudo-Merohedral Twinned Crystalline Family as Solvent-Free Heterogeneous Catalysts

Richard F. D'Vries, Natalia Snejko, Marta Iglesias, Enrique Gutiérrez-Puebla, and M. Angeles Monge*

Instituto de Ciencia de Materiales de Madrid (ICMM-CSIC), C/Sor Juana Inés de la Cruz, n° 3. Cantoblanco 28049 Madrid, Spain

Supporting Information

ABSTRACT: Hydrothermally promoted assembly of the multifunctional 3,5-disulfobenzoic acid (3,5-DSB) ligand with the lanthanide series and the 1,10-phenanthroline as a secondary ligand gives rise to the formation of 2D coordination polymers. The isostructural **RPF-20-Ln** series, with formula $[\mathbf{Ln(3,5\text{-}DSB)(Phen)(H_2O)}]\cdot\mathbf{H_2O}$ (**Ln = Sm, Eu, Gd, Tb, Dy, Ho, Er,** and **Yb**), present pseudomerohedral twinned crystals. The polymeric network consists of uninodal 2D net ($4^3\cdot6^3$) layers perpendicular to the [010] direction. $\pi-\pi$ Stacking interactions between them gives rise to the tridimensional supramolecular framework. The new compounds were tested as catalysts in acid Lewis reactions. A comparative study with other lanthanide MOFs inside the systems Ln/DSB and Ln/DSB/Phen reveals some structural facts that could improve the catalytic behavior of this kind of material.

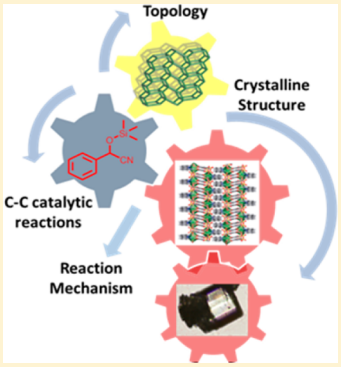

INTRODUCTION

Metal−organic compounds formed by lanthanides are of great interest due to their many possible applications as luminescent or electro-luminescent materials, materials for telecommunications and light emitting diodes, heterogeneous catalysis, magnetic devices, and contrast agents.[1] Many of these properties depend on the structural characteristics of the compound, the nature of the organic component, and the metal. Sulfonate ligands such as 5-sulfoisophthalate,[2] 2-sulfoterephthalic acid,[3] and 2-sulfobenzoic acid[4] have been used for the synthesis of MOFs. The 3,5-disulfobenzoic acid (3,5-DSB) is currently being used as a linker in our group. Compounds with Sc and the first elements of the lanthanide metals row were obtained as three different structural crystalline types and demonstrated interesting catalytic properties.[5] Specifically that of Sc[6] is the first MOF material with the $H_3O_2^-$ species incorporated as the bridging ligand. The versatility in the coordination modes of the 3,5-DSB ligand compared with the tricarboxylic (BTC) one[7] allowed us to obtain compounds with different architectures, topologies, and a high activity in the cyanosilylation reaction,[8] these compounds are also a good option for the application as materials with some particular properties.

In several previous papers[1d,9] it has been shown that, at least with lanthanides, the sulfonic group is not such a weak donor group, as it has usually been considered,[10] thus making their coordination to lanthanides possible (under certain conditions) without needing ancillary ligands. However, the important role that auxiliary chelating ligands, such as 1,10-phenanthroline, play as coordination blocking molecules, allows the MOF dimensionality control, and in many cases the specific material catalytic activity.

In the current study, a new eight member series of 2D MOF materials with Ln, 3,5-disulfobenzoate (3,5-DSB), and 1,10-phenanthroline is presented. The crystallographic resolution of their pseudomerohedral twinned structure, the topological study, and the ability of these compounds as an acid Lewis catalyst in cyanosilylation reactions under solvent-free conditions are also presented.

EXPERIMENTAL SECTION

General Information. All reagents and solvents employed were commercially available and were used as supplied without further purification: 3,5-disulfobenzoic acid, disodium salt (98% Sigma-Aldrich), 1,10-phenanthroline (99% Sigma-Aldrich), $Ln(NO_3)_3$ where Ln = Sm, Gd, Dy, Ho, and Yb (all 99% Strem Chemicals), and $Ln(NO_3)_3$, where Ln = Eu, Er, and Tb (all 99% of Acros Organic). The IR spectra were recorded from KBr pellets in the range of 4000−250 cm^{-1} on a Bruker IFS 66 V/S. The thermogravimetric and differential thermal analyses (TGA-DTA) were performed using Seiko TG/DTA 320U equipment in a temperature range between 25 and 1000 °C in air (100 mL/min flow) and a heating rate of 10 °C/min. A Perkin-Elmer CNHS Analyzer 2400 was employed for the elemental analysis. Powder X-ray diffraction (PXRD) patterns were measured with a Bruker D8 diffractometer, with a step size of 0.02° and an exposure time of 0.5 s/step.

Synthesis. The compounds were synthesized under hydrothermal conditions. The molar composition of the initial reaction mixture was $3,5\text{-}DSB^{3-}$:Ln^{3+}:2 Phen:2400 H_2O.

$[\mathbf{Eu(3,5\text{-}DSB)(Phen)(H_2O)}]\cdot\mathbf{H_2O}$ (**RPF-20-Eu**) was synthesized by addition of $3,5\text{-}DSBNa_2H$ (0.074 g, 0.224 mmol) and phenanthroline (0.07 g, 0.448 mmol) to a solution of $Eu(NO_3)_3\cdot6H_2O$ (0.1 g, 0.224 mmol, and 10 mL of water). The mixture was magnetically

Received: February 14, 2014
Revised: March 11, 2014
Published: March 19, 2014

 © 2014 American Chemical Society dx.doi.org/10.1021/cg5002336 | *Cryst. Growth Des.* 2014, 14, 2516−2521

stirred at room temperature for 15 min. The resultant reaction mixture was then placed into a Teflon-lined stainless steel autoclave and heated at 200 °C for 3 days. After cooling to room temperature, the crystalline product was filtered and washed with water and acetone. The same procedure was used in the synthesis of all **RPF-20-Ln** compounds. Elemental analysis (the small systematic error in the S analysis is probably due to a difficult combustion of this compound sample series) calculated for **RPF-20-Sm** ($C_{38}H_{30}N_4O_{20}S_4Sm_2$): C, 35.30; H, 2.32; N, 4.34; S, 9.91; found: C, 35.46; H, 2.37; N, 4.38; S, 9.51. Calcd for **RPF-20-Eu** ($C_{38}H_{30}N_4O_{20}S_4Eu_2$): C, 35.22; H, 2.32; N, 4.32; S, 9.89; found: C, 35.35; H, 2.27; N, 4.37; S, 9.45. Calcd for **RPF-20-Gd** ($C_{38}H_{30}N_4O_{20}S_4Gd_2$): C, 34.93; H, 2.30; N, 4.29; S, 9.80; found: C, 35.21; H, 2.13; N, 4.37; S, 9.80. Calcd for **RPF-20-Tb** ($C_{38}H_{30}N_4O_{20}S_4Tb_2$): C, 34.84; H, 2.29; N, 4.28; S, 9.78; found: C, 34.99; H, 2.05; N, 4.45; S, 9.54. Calcd for **RPF-20-Dy** ($C_{38}H_{30}N_4O_{20}S_4Dy_2$): C, 34.65; H, 2.28; N, 4.26; S, 9.73; found: C, 34.78; H, 2.14; N, 4.33; S, 9.07. Calcd for **RPF-20-Ho** ($C_{38}H_{30}N_4O_{20}S_4Ho_2$): C, 34.52; H, 2.27; N, 4.24; S, 9.69; found: C, 34.76; H, 2.25; N, 4.24; S, 9.30. Calcd for **RPF-20-Er** ($C_{38}H_{30}N_4O_{20}S_4Er_2$): C, 34.40; H, 2.26; N, 4.22; S, 9.66; found: C, 34.56; H, 2.24; N, 4.26; S, 9.41. Calcd for **RPF-20-Yb** ($C_{38}H_{30}N_4O_{20}S_4Yb_2$): C, 34.11; H, 2.24; N, 4.19; S, 9.57; found: C, 34.21; H, 2.06; N, 4.25; S, 9.05.

Single-Crystal Structure Determination. Pseudomerohedral twinned crystal X-ray data were obtained in a Bruker four circle kappa-diffractometer equipped with a Cu microsource operated at 30 W power (45 kV, 0.60 mA) to generate Cu Kα radiation (λ = 1.54178 Å) and a Bruker VANTEC 500 area detector (microgap technology) at room temperature (296 K). These were explored over a hemisphere of the reciprocal space in a combination of phi and omega scans to reach a resolution of 0.81 Å (71.9270 in θ), using Bruker APEX2 (each exposure of 10 s covered 1° in ω). Unit cell dimensions were determined by a least-squares fit of reflections with $I > 2\ \sigma(I)$. Data were integrated and scaled using SAINT.[11] A semiempirical absorption and scale correction based on equivalent reflection was carried out using SADABS.[11] Space group determination was carried out using XPREP. The structure was solved by direct methods using SHELXS[12] to show all nonhydrogen atoms. Additional cycles of refinement and electron difference maps showed the hydrogen atoms. Refinement was carried out by anisotropic full-matrix least-squares, except for hydrogen atoms which were included with isotropic thermal parameter using SHELXL.[11] Due to the bad quality of the crystals, the merohedral twin and, thus, the strong correlations among atoms, the only crystal that could be anisotropically refined was the one of ytterbium, whose structure was used to eestablish the **RPF-20** structural type as a model to study the whole isostructural lanthanide series by powder X-ray diffraction.

X-ray Powder Diffraction. The X-ray powder diffraction measurements were used to prove the isostructurality of the series and to check the purity of the obtained microcrystalline products by comparison of the experimental results with the simulated pattern obtained from single crystal X-ray diffraction data. The residues for the compounds after TG analyses were analyzed by X-ray powder diffraction and compared with the ICSD patterns reported.

Catalytic Study. The cyanosilylation reaction of aldehydes was carried out at 40 °C. Into a Pyrex-glass screw cap vial (volume: ca. 10 mL), the catalyst 5 mg (2 mol %) and aldehyde (1 mmol) were successively placed in absence of solvent. The reaction was initiated by addition of trimethylsilyl cyanide, TMSCN (1.5 mmol). The reaction mixture was vigorously stirred (800 rpm) at 40 °C under a N_2 atmosphere. The progress of the reaction was monitored by GC analysis. After the reaction was completed, the solid was removed by centrifugation of the reaction mixture. All products (cyanohydrin trimethylsilyl ethers) were identified by comparison of their GC retention times, GC/MS spectra, and/or ^{1}H and ^{13}C NMR spectra with those of authentic data. GC analysis was performed using Konik HRGC 4000B GCMS with a cross-linked (95%)-dimethyl-(5%)-diphenylpolysiloxane (Teknokroma TRB-5MS) column of 30 m.

RESULTS AND DISCUSSION

Structural Description. Details of data collection, refinement, and crystallographic data for the compounds **RPF-20-Yb** are summarized in Table 1. The cell parameters measured for the compounds **RPF-20-Ln** (**Ln** = **Sm**, **Eu**, **Gd**, **Tb**, **Dy**, **Ho**, and **Er**) are presented in Table 2. The coordination environment of the **RPF-20-Ln** compounds is shown in Figure 1.

Table 1. Crystallographic and Refinement Data for RPF-20-Yb

empirical formula	$C_{19}H_{14}N_2O_{9.50}S_2Yb$
formula weight	659.48
temperaturek	571(2)
wavelength	1.54178 Å
crystal system	monoclinic
space group	P2(1)/c
unit cell	a = 18.6903(7) Å
	b = 31.195(1) Å
	c = 6.8692(3) Å
	β = 90.094(3)°
volume	4005.0(3) Å^3
Z	4
density	2.187 Mg/m^3
absorption coefficient	11.164 mm^{-1}
F(000)	2560
crystal size	0.07 × 0.05 × 0.03 mm^3
θ range	1.42 to 71.93°
index ranges	(−21,22) (−22,36) (−8,8)
reflections collected	47538
independent reflections	7299 [R(int) = 0.0573]
data/restraint/parameters	7299/0/598
Goodness-of-fit on F^2	1.032
R indices [$I > 2\sigma(I)$]	$R1$ = 0.0457, $wR2$ = 0.1078
R indices (all data)	$R1$ = 0.0554, $wR2$ = 0.1139
largest difference peak, hole	1.479 and −1.999 e Å^{-3}

Table 2. Cell Parameters for RPF-20

	a (Å)	b (Å)	c (Å)	β (deg)	V (Å^3)
Sm	18.902(5)	31.537(7)	6.971(2)	90.357(4)	4155(2)
Eu	18.874(6)	31.480(9)	6.954(2)	90.058(5)	4132(2)
Gd	18.774(4)	31.370(6)	6.919(1)	90.298(4)	4075(1)
Tb	18.786(5)	31.410(7)	6.923(2)	90.578(5)	4085(3)
Dy	18.780(2)	31.348(3)	6.909(1)	89.997(2)	4067(9)
Ho	18.749(2)	31.296(4)	6.892(1)	90.014(5)	4044(1)
Er	18.759(3)	31.290(5)	6.894(1)	90.267(3)	4046(1)

[Ln(3,5-DSB)(Phen)(H_2O)]·H_2O, RPF-20-Ln (**Ln** = **Sm**, **Eu**, **Gd**, **Tb**, **Dy**, **Ho**, **Er**, and **Yb**) is a series of isostructural compounds whose crystals are polisynthetically twinned. The initial data collection gave an orthorhombic cell with space group *Pbca*. The structure presented several U_{ij} determinants negative and high R values, which revealed a twin problem. Since the β angle was very close to 90°, the presence of a pseudomerohedral twin was very likely, suggesting that the emulated metric symmetry is higher than that of the crystal. The $|E^2 - 1|$ low values of 0.844, 0.782, 0.852, for **RPF-20-Eu**, **RPF-20-Gd**, and **RPF-20-Yb** (from several not very fruitful data collections), respectively,[11] also suggested the twin; consequently, by lowering the symmetry to the $P2_1/c$ group

dx.doi.org/10.1021/cg5002336 | Cryst. Growth Des. 2014, 14, 2516−2521

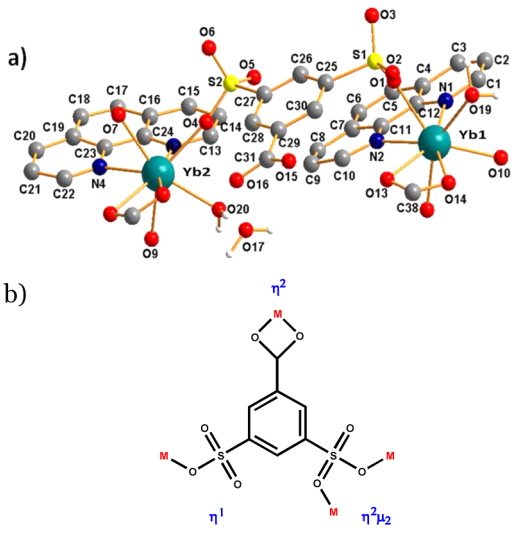

Figure 1. (a) Ln coordination environment and (b) 3,5-DSB ligand link modes in **RPF-20**.

and the twin law with matrix (1 0 0, 0 −1 0, 0 0 −1), the structure was refined and the structural type established. Distances and angles for the Yb compound are in Section S1 of the Supporting Information.

The **RPF-20** structure consists of two crystallographically independent lanthanide cations, which are octa-coordinated to five oxygen atoms of the 3,5-DSB, one water molecule, and two chelating phenantroline nitrogen atoms in a LnO_6N_2 trigonal square face bicapped prism[12] (Figure 2). The 3,5-DSB anion acts as a tetratopic ligand with the carboxylate group in the chelate mode (η^2), one of the sulfonic groups, which connects the lanthanide cations along the [001] direction, in the anti−anti ($\eta^2\mu_2$) mode, and the other, only coordinated by one oxygen atom in the η^1 syn mode, connects them in the [100] direction to give rise to extended layers perpendicular to the

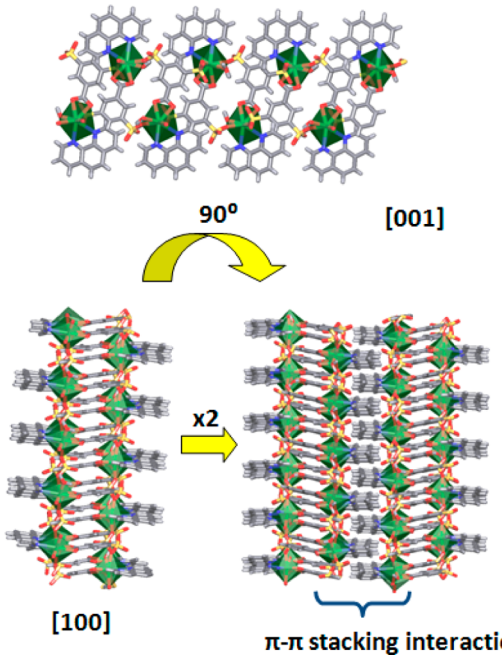

Figure 2. View of the layers along the [001] and [100] directions and the $\pi-\pi$ stacking interactions for **RPF-20-Ln**.

[010] direction. The three-dimensional supramolecular structure is formed through a $\pi-\pi$ stacking interaction among phenanthroline rings (Figure 2) along the [001] direction with distances among rings 3.5897(5) Å for **RPF-20-Yb**.

It should be noted that although the hydrothermal synthetic procedure used for **RPF-20** (**Sm**, **Eu**, **Gd**, **Tb**, **Dy**, **Ho**, **Er**, and **Yb**) is very similar to that of **RPF-18** (**La**, **Pr**) and **RPF-19** (**Nd**) obtained previously[5b] and they have similar formulas (the difference consists only in the presence of coordinated and occluded water molecules in the structure of **RPF-20**); the **RPF-18**, **RPF-19**, and **RPF-20** possess different structures and topology, which is due to the lanthanide contraction along the lanthanide series. In the comparison of structures **RPF-18**, **RPF-19**, and **RPF-20**, changes are seen not only in the coordination environment of the central REE cation but also in the 3,5-DSB ligand link modes.

Topological Analysis. The structure simplification of the 0-connected ligands (phenanthroline and water) allows us to see that the lanthanide cations are joined by four 3,5-DSB molecules and that each ligand is linked to four metallic cations. The topological analysis reveals that the structure is composed by uninodal 4-connected layers in the plane (101). This topology has a point (Schläfli) symbol ($4^3\cdot6^3$) and is described as SP 2-periodic net (6,3)Ia, TOPOS (Figure 3).[13] It can be

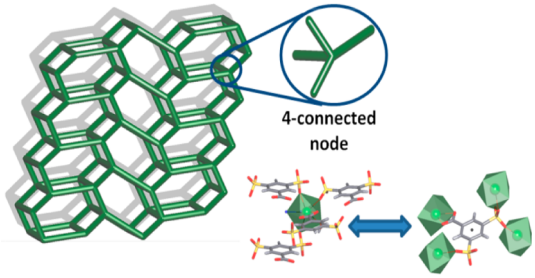

Figure 3. Schematic description of the 4-connected bidimensional net ($4^3\cdot6^3$) topology.

observed that the layers are related by a glide plane so that each layer is displaced one-half along the [001] direction. This arrangement allows the layer interdigitation and forces the phenanthroline aromatic ring interactions (Figure 2).

X-ray Powder Diffraction. The powder patterns for all the compounds were obtained and compared with the simulated pattern of the **RPF-20** calculated on the basis of the determined crystal structure. They show the isostructurality and purity of the sample bulks (Section S2 of the Supporting Information).

IR Spectra. In **RPF-20-Ln** we can observe that the IR profiles of all the compounds are similar. The C−H vibrations in aromatic rings of phenanthroline and 3,5-DSB ligands are assigned to the bands around ∼3078−3117 cm^{-1}. The O−H vibrations of the free and coordination water molecules are present in the region around ∼3510−3301 cm^{-1}. The ν_{as}(OCO) is observed at ∼1628 cm^{-1} and the band associated with the symmetric mode at ∼1355 cm^{-1}. S−O vibrations are observed at ∼1160−1030 cm^{-1}.[14] In this region we have also found four bands characteristic of the bridge bidentate sulfonate group ($\eta^2\mu_2$).[14] The bands around ∼415−430 cm^{-1} are assigned to M−O vibrations, and the band observed around ∼268 cm^{-1} corresponds to M−N vibrations (Section S3 of the Supporting Information).

Thermal Study. The thermograms of **RPF-20-Ln** compounds present a mass loss around ∼150 °C, which

dx.doi.org/10.1021/cg5002336 | Cryst. Growth Des. 2014, 14, 2516−2521

corresponds to the loss of two physisorbed water molecules and two coordinated water molecules. X-ray thermo-diffraction patterns (Sections S4 and S5 of the Supporting Information) show a reversible shift of the spectrum in all the cases, which corresponds to the [**Ln(3,5-DSB)(Phen)(H_2O)]·H_2O** < = > [**Ln(3,5-DSB)(Phen)**] equilibrium within the temperature range.

The total decomposition of the compounds begins at ∼460 °C (Section S8 of the Supporting Information). The final product for the **Yb** compound is the ytterbium oxide.[15] The compounds of **Er, Ho**, and **Dy** present as decomposition product mixtures of metallic oxides and oxysulfates (Section S4 of the Supporting Information).[16] The compounds of **Sm, Eu, Gd**, and **Tb** decompose forming rare earth oxysulfates. All the decomposition products were confirmed by comparing observed powder X-ray diffraction patterns with those reported in the ICSD database (Section S4 of the Supporting Information).

Catalytic Study. Metal−organic frameworks are important heterogeneous catalysts for Lewis acid reactions due to their unique reactivity and selectivity under mild reaction conditions.[17] One of the most important acid Lewis catalyzed reactions is the cyanosylilation reaction; in this reaction, the C−C bond-forming is promoted by the activation of the carbonyl carbon and the addition of the nitrile group to give rise to the silylcyanide ester, a precursor of the cyanohydrines.[7b,18] **RPF-20-Ln** catalysts own coordinated water molecules susceptible of being displaced, and thus of generating the catalytically active species;[5b,8] consequently, they were tested for cyanosilylation of benzaldehyde with trimethylsilyl cyanide, under solvent-free conditions and low catalyst load (40 °C, inert atmosphere, 2 mol % catalyst), resulting in 2-phenyl-2-(trimethylsilyl) acetonitrile as the only product.

First of all, the reactivity of the **RPF-20-Ln** series (**Ln** = **Sm, Dy**, and **Yb**) was studied, finding that the **RPF-20-Sm** catalyst yields the product almost quantitatively after 3 h, while the yields for **Dy** and **Yb** catalysts were lower than 70 and 50%, respectively (Figure 4).

Second, in order to confirm that the **RPF-20-Yb** catalytic behavior (apparent deactivation and lower activity) was only due to the small lanthanide size and to get a deeper knowledge of the reaction mechanism, three more experiments were carried out: (i) the influence of the temperature on the activity of the **RPF-20-Yb** was analyzed to calculate the apparent activation energy (Section S7 of the Supporting Information). It resulted in $E_a \approx 5.27$ kcal/mol, a normal value for this kind of reaction, which rules out a possible catalyst deactivation. (ii) The reaction was performed after heating the bulk at 150 °C for one hour **RPF-20-Yb-dry** (from now on) to force the loss of coordinated water molecules. The catalytic activity of RPF-20-Yb-dry increases 30% compared with RPF-20-Yb, which indicates that the dehydrated form is the catalytically active species. (iii) The recovered **RPF-20-Yb** was used in a second cycle, obtaining an intermediate yield between the dehydrated form and the as-synthetized one (Figure 5). (iv) DSC analyses of the catalyst before and after the first cycle of the catalytic reaction were performed.

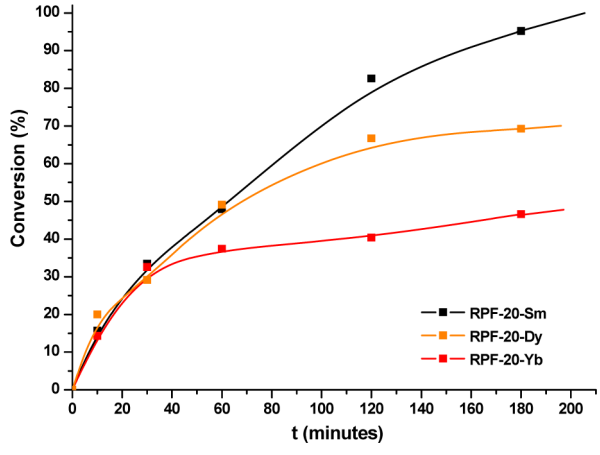

Figure 4. Kinetic profiles of the compounds **RPF-20-Ln** (**Ln** = **Sm, Dy**, and **Yb**) for the cyanosilylation reaction.

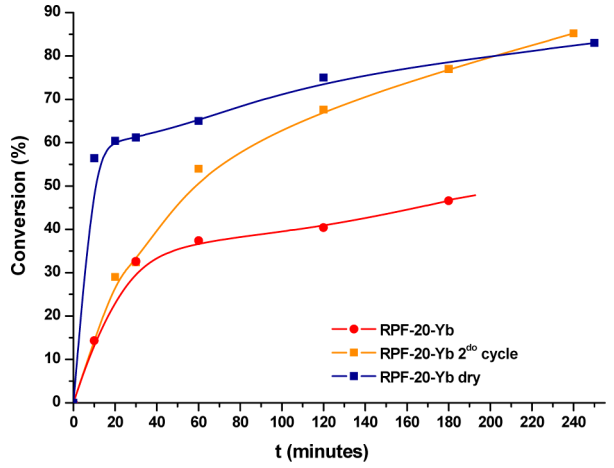

Figure 5. Comparison of catalytic profiles of the compound **RPF-20-Yb-dry**, **RPF-20-Yb**, and **RPF-20-Yb-2nd cycle**.

Figure 6 shows the loss of water at 150 °C (in blue) and the absence of it after the first run of the catalytic (in black); the small peak (notice the different scale) that appears around 130 °C can be attributed to some residual substrate interaction.

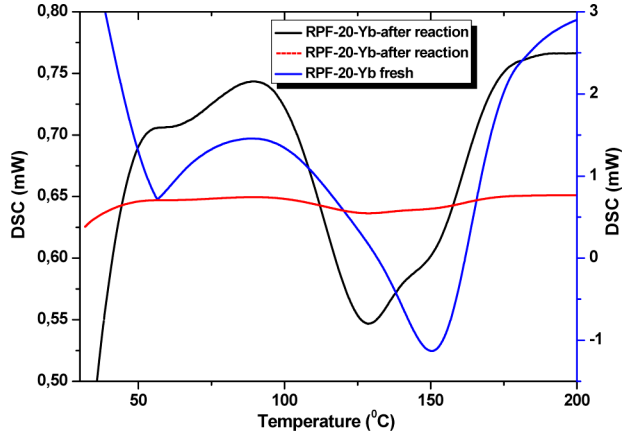

Figure 6. DSC analysis for **RPF-20-Yb** fresh and after the catalytic reaction. Blue and red curves represents data in the same scale (right-side scale) and black corresponds to the red one amplified in a scale multiplied by 15 (left-side scale).

These results evidence that for **RPF-20-Yb**, the compound with the smallest cation of the series, the displacement of the water molecule is essential to form the catalytically active

dx.doi.org/10.1021/cg5002336 | Cryst. Growth Des. 2014, 14, 2516−2521

species, while in the case of **RPF-20-Sm**, with a larger cation, and thus with the possibility of increasing its coordination number when the reaction starts, the yield is nearly stoichiometric. All in all, the catalytic behavior along the series allows us to propose the mechanism shown in Figure 7, in

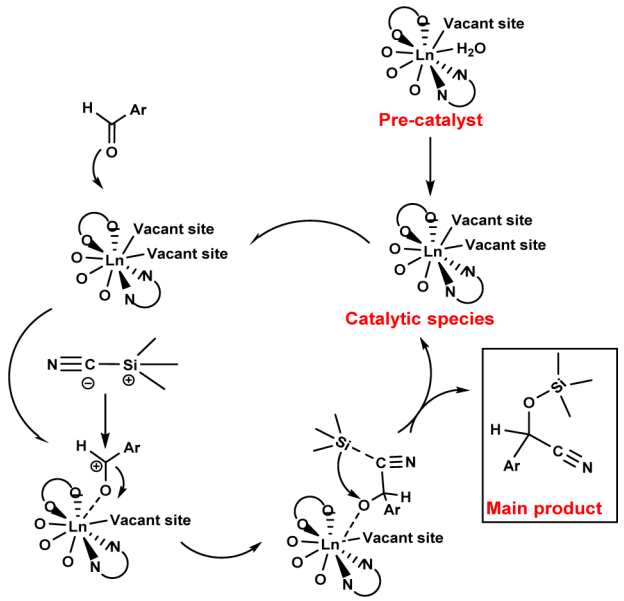

Figure 7. Proposed mechanism for **RPF-20-Ln**-catalyzed cyanosilylation of aldehydes.

which the active species formation goes from the displacement of the coordinated water molecule at the Ln series end (**RPF-20-Yb**) (Figure 7) to the increasing coordination number at its beginning (**RPF-20-Sm**), passing through combinations of both paths, depending on the lanthanide size.

It is worth comparing the results of this work with those previously obtained for the first lanthanide elements with different structure type (**RPF-18-Pr** and **RPF-19-Nd**)[5b] and with those without ancillary ligands, where the series adopts three different structural types (**RPF-21**, **RPF-22**, and **RPF-23**).[8] From Table 3 data, some observations should be done.

Table 3. RPF Compounds As Catalysts for Cyanosilylation of Benzaldehyde

compound	TOF (h^{-1})	coordination index	topology
RPF-18-Pr	6.48	8	SP 2-periodic net (6,3)IIa topology
RPF-19-Nd	12.94	9	kgd
RPF-20-Sm	23.6	8	SP 2-periodic net (6,3)Ia
RPF-21-Pr	78.8	9	sql/Shubnikov tetragonal plane
RPF-22-Pr	10.2	8	SP 2-periodic net (6,3)IIa
RPF-23-Pr	13.8	8,9	new topology

The first thing that strikes is the higher **RPF-21-Pr** TOF value. After examining the **RPF-21** structure the explanation clearly comes out. This compound aside from possessing five coordinated water molecules (per Ln cation) susceptible of being displaced also owns one of the DSB sulfonate groups of each ligand uncoordinated, which increases the acidity of the catalyst, and, thus, its reactivity. Apart from this latter, we can see that the current **RPF-20-Sm** is the most active, without regard to the coordination index, the net dimensionality, or topology. Altogether, this seems to indicate that the use of a blocking chelating ligand like the 1,10-phenanthroline favors the reactivity of the catalyst. Accordingly, to improve the reactivity of these lanthanide catalysts, the design of new ones should be addressed toward obtaining the Ln-MOFs, in which the lanthanides are coordinated to displaceable water molecules, in order to create the active species (specially for small lanthanides), and to blocking chelating ligands that avoid the total coordination of the DSB ligand, and thus, force the possibility of having noncoordinated sulfonate groups in the framework.

The recyclability and heterogeneity of the catalyst was demonstrated in at least four catalytic cycles for the **RPF-20-Ln** catalysts, using the same reaction conditions (Figure 8). The

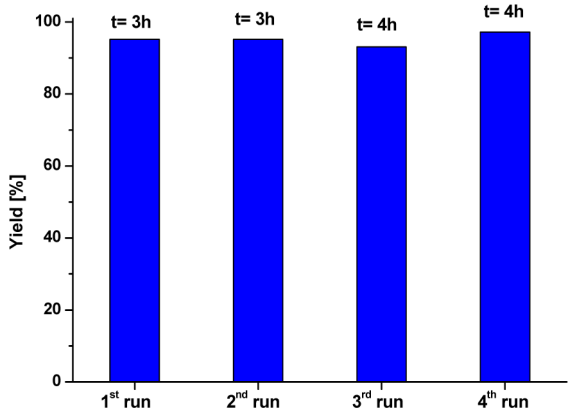

Figure 8. Recycling experiments for cyanosilylation of benzaldehyde catalyzed by **RPF-20-Sm**.

catalysts were removed from the reaction media, washed, and analyzed to confirm the conservation of the structure by powder X-ray diffraction (S8 of the Supporting Information). It was observed that activity, structure, and crystallinity were unaltered after the reaction, demonstrating the heterogeneous nature of the catalyst.

CONCLUSION

The isostructural **RPF-20-Ln** series, with formula [**Ln(3,5-DSB)(Phen)(H_2O)**]·**H_2O** (**Ln = Sm, Eu, Gd, Tb, Dy, Ho, Er,** and **Yb**) has been obtained and presents pseudomerohedral twinned crystals. The polymeric network consists of uninodal 2D net ($4^3 \cdot 6^3$) layers. $\pi-\pi$ Stacking interactions between them gives rise to the tridimensional supramolecular framework. The series behavior as catalysts in acid Lewis reactions allows us to propose a mechanism in which the active species formation goes from the displacement of the coordinated water molecule at the Ln series end (**RPF-20-Yb**) to the increasing coordination number at its beginning (**RPF-20-Sm**), passing through combinations of both paths depending on the lanthanide size. A comparative study with other lanthanide MOFs inside the systems Ln/DSB and Ln/DSB/Phen reveals some structural facts that could improve the catalytic behavior of this kind of material.

dx.doi.org/10.1021/cg5002336 | *Cryst. Growth Des.* 2014, 14, 2516−2521

■ ASSOCIATED CONTENT

Supporting Information

Selected bond lengths and hydrogen bonds and angles, experimental X-ray powder patterns, X-ray powder thermo-diffraction pattern, X-ray powder patterns for RPF-20-Ln compounds after TG analysis and before and after catalytic reactions for the RPF-20-Ln compounds. DSC analysis for the compound **RPF-20-Yb** before and after catalytic reaction and kinetic profiles of the compound **RPF-20-Yb-dry**, **RPF-20-Yb**, and **RPF-20-Yb-2nd run**. This material is available free of charge via the Internet at http://pubs.acs.org. CCDC reference number 986912 contains the supplementary crystallographic data for this paper. This data can be obtained free from the Cambridge Crystallographic Data Centre via www.ccdc.cam.ac.uk/data_request/cif.

■ AUTHOR INFORMATION

Corresponding Author

*E-mail: amonge@icmm.csic.es.

Notes

The authors declare no competing financial interest.

■ ACKNOWLEDGMENTS

R.D. acknowledges a FPI scholarship from Spanish Ministry of Science and Innovation (MICIN) and Fondo Social Europeo from the EU. This work has been supported by the Spanish MCYT Project MAT2010-17571, Consolider-Ingenio CSD2006-2010, MAT2011-29020-C02-02, PHAMA S2009/MAT-1756 Comunidad Autónoma de Madrid.

■ REFERENCES

(1) (a) Bünzli, J.-C. G.; Comby, S.; Chauvin, A.-S.; Vandevyver, C. D. B. *J. Rare Earths* **2007**, *25*, 257. (b) Choppin, G. R.; Peterman, D. R. *Coord. Chem. Rev.* **1998**, *174*, 283. (c) Gándara, F.; Andrés, A. d.; Gómez-Lor, B.; Gutiérrez-Puebla, E.; Iglesias, M.; Monge, M. A.; Proserpio, D. M.; Snejko, N. *Cryst. Growth Des.* **2008**, *8*, 378. (d) Gándara, F.; García-Cortés, A.; Cascales, C.; Gómez-Lor, B.; Gutiérrez-Puebla, E.; Iglesias, M.; Monge, A.; Snejko, N. *Inorg. Chem.* **2007**, *46*, 3475. (e) Rieter, W. J.; Taylor, K. M. L.; An, H.; Lin, W.; Lin, W. *J. Am. Chem. Soc.* **2006**, *128*, 9024. (f) D'Vries, R. F.; Alvarez-Garcia, S.; Snejko, N.; Bausa, L. E.; Gutierrez-Puebla, E.; de Andres, A.; Monge, M. A. *J. Mater. Chem. C* **2013**, *1*, 6316. (g) Harbuzaru, B. V.; Corma, A.; Rey, F.; Atienzar, P.; Jordá, J. L.; García, H.; Ananias, D.; Carlos, L. D.; Rocha, J. *Angew. Chem., Int. Ed.* **2008**, *47*, 1080.

(2) (a) Liu, Q.-Y.; Xu, L. *Eur. J. Inorg. Chem.* **2005**, *2005*, 3458. (b) Wang, Z.; Ströbele, M.; Zhang, K.-L.; Meyer, H. J.; You, X.-Z.; Yu, Z. *Inorg. Chem. Commun.* **2002**, *5*, 230.

(3) Schlichte, K.; Kratzke, T.; Kaskel, S. *Microporous Mesoporous Mater.* **2004**, *73*, 81.

(4) Xiao, H.-P.; Zheng, Y.-X.; Liang, X.-Q.; Zuo, J.-L.; You, X.-Z. *J. Mol. Struct.* **2008**, *888*, 55.

(5) (a) Li, X.; Wang, C.-Y.; Hu, H.-M. *Inorg. Chem. Commun.* **2008**, *11*, 345. (b) D'Vries, R. F.; Iglesias, M.; Snejko, N.; Gutiérrez-Puebla, E.; Monge, M. A. *Inorg. Chem.* **2012**, *51*, 11349.

(6) D'Vries, R. F.; de la Peña-O'Shea, V. A.; Snejko, N.; Iglesias, M.; Gutiérrez-Puebla, E.; Monge, M. A. *J. Am. Chem. Soc.* **2013**, *135*, 5782.

(7) (a) Gustafsson, M.; Bartoszewicz, A.; Martín-Matute, B.; Sun, J.; Grins, J.; Zhao, T.; Li, Z.; Zhu, G.; Zou, X. *Chem. Mater.* **2010**, *22*, 3316. (b) Horike, S.; Dincá, M.; Tamaki, K.; Long, J. R. *J. Am. Chem. Soc.* **2008**, *130*, 5854.

(8) D'Vries, R. F.; de la Peña-O'Shea, V. A.; Snejko, N.; Iglesias, M.; Gutiérrez-Puebla, E.; Monge, M. Á. *Cryst. Growth Des.* **2012**, *12*, 5535.

(9) (a) Snejko, N.; Cascales, C.; Gomez-Lor, B.; Gutierrez-Puebla, E.; Iglesias, M.; Ruiz-Valero, C.; Monge, M. A. *Chem. Commun.* **2002**, 1366. (b) Gándara, F.; Gutiérrez-Puebla, E.; Iglesias, M.; Proserpio, D. M.; Snejko, N.; Monge, M. A. *Chem. Mater.* **2009**, *21*, 655. (c) Gándara, F.; Gutiérrez-Puebla, E.; Iglesias, M.; Snejko, N.; Monge, M. A. *Cryst. Growth Des.* **2010**, *10*, 128. (d) Perles, J.; Snejko, N.; Iglesias, M.; Monge, M. A. *J. Mater. Chem.* **2009**, *19*, 6504. (e) Medina, M. E.; Platero-Prats, A. E.; Snejko, N.; Rojas, A.; Monge, A.; Gándara, F.; Gutiérrez-Puebla, E.; Camblor, M. A. *Adv. Mater.* **2011**, *23*, 5283. (f) Monge, A.; Gandara, F.; Gutierrez-Puebla, E.; Snejko, N. *CrystEngComm* **2011**, *13*, 5031.

(10) (a) Cai, J. *Coord. Chem. Rev.* **2004**, *248*, 1061. (b) Chen, C.-H.; Cai, J.; Liao, C.-Z.; Feng, X.-L.; Chen, X.-M.; Ng, S. W. *Inorg. Chem.* **2002**, *41*, 4967.

(11) Müller, P., Herbst-Irmer, R., Spek, A., Schneider, T., Sawaya, M. *Crystal Structure Refinement: A Crystallographer's Guide to SHELXL*; Oxford University Press Inc.: New York, 2006.

(12) Connelly, N. G.; Damhus, T.; Hartshorn, R. M.; Hutton, A. T. *Nomenclature of Inorganic Chemistry - IUPAC Recommendations 2005*; RSC Publishing: Cambridge, U.K., 2005.

(13) Blatov, V. A.; Shevchenko, A. P. *TOPOS*, version 4.0; Samara State University: Samara, Russia, 2010.

(14) *Infrared and Raman Spectra of Inorganic and Coordination Compounds*, 6th ed.; Nakamoto, K., Ed.; John Wiley & Sons, Inc.: Hoboken, NJ, 2009.

(15) Ben Farhat, L.; Amami, M.; Hlil, E. K.; Ben Hassen, R. *J. Alloys Comp.* **2009**, *479*, 594.

(16) Hartenbach, I.; Schleid, T. *Z. Anorg. Allg. Chem.* **2002**, *628*, 2171.

(17) (a) Kobayashi, S.; Sugiura, M.; Kitagawa, H.; Lam, W. W. L. *Chem. Rev.* **2002**, *102*, 2227. (b) Kobayashi, S.; Mori, Y.; Yamashita, Y. In *Comprehensive Coordination Chemistry II*; McCleverty, J. A., Meyer, T. J., Eds.; Pergamon: Oxford, 2003. (c) Corma, A.; García, H.; Llabrés i Xamena, F. X. *Chem. Rev.* **2010**, *110*, 4606.

(18) (a) Ohmori, O.; Fujita, M. *Chem. Commun.* **2004**, 1586. (b) Hong, D.-Y.; Hwang, Y. K.; Serre, C.; Férey, G.; Chang, J.-S. *Adv. Funct. Mater.* **2009**, *19*, 1537. (c) Hasegawa, S.; Horike, S.; Matsuda, R.; Furukawa, S.; Mochizuki, K.; Kinoshita, Y.; Kitagawa, S. *J. Am. Chem. Soc.* **2007**, *129*, 2607. (d) Baleizão, C.; Gigante, B.; García, H.; Corma, A. *Tetrahedron* **2004**, *60*, 10461.